

Role of a Cumulus Parameterization Scheme in Simulating Atmospheric Circulation and Rainfall in the Nine-Layer Goddard Laboratory for Atmospheres General Circulation Model

Y. C. SUD, WINSTON C. CHAO, AND G. K. WALKER*

Laboratory for Atmospheres, NASA/Goddard Space Flight Center, Greenbelt, Maryland

(Manuscript received 26 February 1991, in final form 9 August 1991)

ABSTRACT

A coarse ($4^\circ \times 5^\circ \times 9$ -sigma level) version of the Goddard Laboratory for Atmospheres (GLA) General Circulation Model (GCM) was used to investigate the influence of a cumulus convection scheme on the simulated atmospheric circulation and hydrologic cycle. Two sets of integrations, each containing an ensemble of three summer (June, July, and August) simulations, were produced. The first set, containing control cases, included a state-of-the-art cumulus parameterization scheme in the GCM; whereas the second set, containing experiment cases, used the same GCM but without the cumulus parameterization. All simulations started from initial conditions that were taken from analysis of observations for three consecutive initial times that were only 12 h apart, beginning with 0000 UTC 19 May 1988. The climatological boundary conditions—sea surface temperature, snow, ice, and vegetation cover—were kept exactly the same for all the integrations. The ensemble sets of control and experiment simulations are compared and differentially analyzed to determine the influence of a cumulus convection scheme on the simulated circulation and hydrologic cycle.

The results show that cumulus parameterization has a very significant influence on the simulated circulation and precipitation. The influence is conspicuous in tropical regions, interior of continents in the Northern Hemisphere, and some oceanic regions. The upper-level condensation heating over the intertropical convergence zone (ITCZ) is much smaller for the experiment simulations as compared to the control simulations; correspondingly, the Hadley and Walker cells for the control simulations are also weaker and are accompanied by a weaker Ferrel cell in the Southern Hemisphere. The rainfall under the rising branch of the southern Ferrel cell (at about 50°S) does not increase very much because boundary-layer convergence poleward reduces the local evaporation. Overall, the difference fields show that experiment simulations (without cumulus convection) produce a cooler and less energetic atmosphere. The vertical profile of the zonally averaged diabatic heating also shows large differences in the tropics that are physically consistent with accompanying differences in circulation. Despite producing a warmer and wetter planetary boundary layer (PBL) in the tropics (20°S – 20°N), the control simulations also produce a warmer but drier 400-mb level. The moisture transport convergence fields show that while only the stationary circulation is affected significantly in the PBL, both the stationary and eddy moisture transports are altered significantly in the atmosphere above the PBL. These differences not only reaffirm the important role of cumulus convection in maintaining the global circulation, but also show the way in which the presence or absence of a cumulus parameterization scheme can affect the circulation and rainfall climatology of a GCM.

1. Introduction

As a consequence of recent development-cum-analysis work of Sud et al. (1991) on the cumulus parameterization in the 4° latitude \times 5° longitude \times 9-sigma level version of the Goddard Laboratory for Atmospheres (GLA) General Circulation Model (GCM)¹,

* Centel Federal Services Incorporated.

¹ The physical parameterizations of the 9-layer GLA GCM are quite different from those of the current 17-layer GLA GCM that was initially developed by Max Suarez as the Phoenix model and is currently being further developed by Michael Fox-Rabinovitz and used by several scientists in the branch as the new GLA GCM.

Corresponding author address: Dr. Yogesh G. Sud, NASA/Goddard Space Flight Center, Code 911, Greenbelt, MD 20771.

it became evident that more could be learned about the extent of the role of cumulus convection by comparing simulation experiments with and without cumulus convection. The first intensive study of this kind was conducted by Donner et al. (1982) with the Australian Numerical Meteorology Research Center (ANMRC) GCM. They show that, with the Kuo's (1974) cumulus convection scheme, the ANMRC GCM produced a warmer and wetter upper troposphere and a cooler and drier lower troposphere including the boundary layer, particularly in the tropics. This is understandable because Kuo's (1974) cumulus parameterization is designed to remove moisture from the planetary boundary layer (PBL) and use a part of it to produce condensation warming, and the rest to moisten aloft. Cooling in the PBL presumably is the outcome of evaporation of large-scale rain because in the Kuo's scheme, there is no provision for cooling by

evaporation of falling rain or downdrafts. Donner et al. (1982) also found that cumulus convection increased the static stability of the tropical troposphere and thereby reduced the strength of the Hadley cell. More recently, Ose et al. (1989) have conducted simulation studies, with the Meteorological Research Institute (MRI) GCM, to understand the role of cumulus convection in maintaining the Hadley cell, and the zonal-mean structure of heating. They assumed aquaplanet under equinox conditions for the experiment and found that significant changes in circulation can be produced by altering the cumulus entrainment parameters of the Arakawa-Schubert (1974) cumulus parameterization scheme (ASCP). For the limiting cases of entrainment, their experiments represent a comparison of no cumulus convection simulations with that of a realistic cumulus convection simulation. However, some major differences appear between the inferences of Ose et al. (1989) and Donner et al. (1982). We recognize that the most important differences between these studies emanate largely from differences in the GCMs, particularly the treatment of cumulus convection. In fact, Donner et al. (1982) state unequivocally that the results of their investigation may be parameterization scheme dependent. Specifically mentioned is the role of four contributing factors: (i) vertical flux convergence of entropy and temperature, (ii) cumulus friction, (iii) GCM-cumulus parameterization interaction, and (iv) cloud-radiative feedback effects of cumulus clouds.

As regards to simulations with the GLA GCM, it is stated at the outset that despite several improvements in the moist- and dry-convective processes, as described in section 2 and discussed in more detail in Sud and Walker (1990), the model has continued to produce an overly vigorous hydrological cycle particularly in the tropics; and, before attempting to solve this problem by improving the cumulus scheme, it is useful to determine the role, as well as limitations, of a cumulus parameterization scheme in maintaining and/or modulating the global hydrologic cycle. This is our primary motivation for conducting numerical experiments comparing simulations produced with and without cumulus convection. In other words, if the model were to continue to produce an excessively vigorous hydrologic cycle, even in the absence of a cumulus convection scheme, it can be safely inferred that the problem of excessive tropical evaporation and precipitation is not directly caused by too efficient a cumulus scheme.

Recently, Geller et al. (1988) conducted simulation studies of the winter-season circulation anomalies in response to the 1982/83 El Niño event with the GLA GCM and showed that the choice of a cumulus scheme can make a significant difference for the atmospheric circulation and rainfall anomaly predictions; that result also provided an additional impetus for the present investigation. Our primary focus here is on those regions of the world that exhibit a considerable amount

of moist convection in the summer months of June, July, and August.

This paper analyzes results of an investigation that is similar to that of Donner et al. (1982), except for the following differences: (i) the Sud and Walker (1990) version of the nine-layer GLA GCM (Kalnay et al. 1983), which has undergone a series of improvements in the physical parameterizations over the last 7 years, was employed for the study; (ii) instead of employing only one case of 40-day-long simulations, an ensemble of three sets of 105-day-long integrations are used in this study—this has enabled us to obtain an estimate of the statistical significance of the differences between the simulations with and without cumulus convection.

As compared to Ose et al. (1989), who used aquaplanet conditions, the present study uses realistic initial and earth surface boundary conditions. Moreover, the physical parameterizations of moist-convective processes, dry-convective adjustment, and cloud-radiation interaction are significantly different from that of MRI GCM, even though both models contain the same Arakawa-Schubert (1974) cumulus parameterization scheme.

2. Particulars of the GCM

The $4^\circ \times 5^\circ \times 9$ -sigma level GLA GCM employed for this study is an improved version of the Goddard Laboratory for Atmospheric Studies (GLAS) GCM documented by Kalnay et al. (1983). Consequently, the rainfall climatology of the model is much more realistic than ever before (see Sud et al. 1991 and Sud and Molod 1988 for further details). However, the sea surface temperatures (SSTs) and initial soil moisture, as well as the snow and ice boundaries, are the same as in Kalnay et al. (1983). The model parameterizations include the Arakawa-Schubert (1974) cumulus parameterization scheme that requires a threshold value of 90% relative humidity at the cloud base for the onset of moist convection and supersaturation condition that is above 100% relative humidity, for the production of large-scale condensation; a formulation of fractional cloudiness for nonprecipitating clouds following Slingo and Ritter (1986); a scheme for calculating the area of detraining cumulus anvils for obtaining raining-cloud-area fractions; Sud and Molod (1988) parameterization of evaporation from falling raindrops; a dry-convective adjustment that mixes air masses of dry-convectively unstable layers to equalize their potential temperature, specific humidity, and momentum without violating conservation laws. The simple biosphere model (SiB) of Sellers et al. (1986) is used to parameterize land surface processes. It uses aerodynamic resistances from the surface layer and PBL stability-dependent drag and heat flux parameters of Sud and Abeles (1980) based on curve-fit data. The model also contains some additional modifications of

Sud et al. (1991) to ASCP, which were found to improve the tropical simulations. The solar radiation of the model is by Lacis and Hansen (1974), except for recent modifications by Chou (1986) for water vapor calculation, and by Sud and Walker (1990) for radiative effects of climatological distribution of dust aerosols. The longwave radiation is due to Wu (1980). It was further modified to handle cloud-radiation interaction effects of fractional cloudiness, following Wu and Susskind's (1990) studies involving comparison of outgoing longwave radiation (OLR) calculations based on High-Resolution Infrared Sounder 2-Microwave Sounding Unit (HIRS2-MSU) retrieved fields of temperature, humidity, and cloud-top pressures with the corresponding observations from the earth radiation budget (ERB) instruments on *Nimbus-7*. For cloud-radiation interactions, all fractional clouds are assumed to be randomly distributed in the vertical. However, for solar radiation the optical thickness of clouds is externally prescribed as a function of sigma layer, whereas clouds are assumed to be opaque to longwave radiation. A review of the influence of all these improvements in physical parameterizations on the simulated circulation and rainfall climatology is given in Sud and Walker (1990). This model does not contain gravity-wave drag parameterization, cumulus downdrafts, and turbulence-driven moisture, heat, and momentum flux transports by Helfand (1986).

3. Design of the experiment

Cumulus convection has been recognized as one of the most important physical parameterizations of a GCM. Consequently, lack of realistic rainfall simulation by GCMs, particularly in convectively active regions, has been attributed to inaccuracies and uncertainties of the cumulus parameterization scheme(s). In a previous study, Sud et al. (1991) have shown how the GLA GCM's simulations are sensitive to several free parameters in the ASCP, which is the current cumulus scheme of the model. In order to determine the overall role of this cumulus scheme, an ensemble of three control cases were run with the best version of the ASCP in the GLA GCM; then a similar ensemble of three anomaly cases, in which the ASCP was suppressed, were run. The 3-month period of June–August was chosen for analysis. The summer period is particularly suitable because convection plays a dominant role in maintaining the circulation and rainfall climatology of major continents in the Northern Hemisphere. Although, three different initial conditions for 0000 UTC 19 May 1988, 1200 UTC 19 May 1988, and 0000 UTC 20 May 1988 were used to produce the ensemble of three simulations, the initial conditions are unimportant because we are examining the climate simulation of the model. An obvious reason for using an ensemble of three simulations is to isolate the statistically significant features of differences in the cir-

ulation and hydrologic cycle. Indeed, only the last 92 days of the integrations, representing June–August simulations, were analyzed; this allowed a period of 10–11 days for initial adjustment of the model. The primary purpose of this exercise is to compare the model's circulation and rainfall climatologies with and without a state-of-the-art cumulus convection scheme (ASCP) in the model. Thus, we can isolate the influence of ASCP on the simulations as well as develop an overall understanding of the role of cumulus processes in the atmosphere.

A usual caution for interpreting results of such a study is that the role of a cumulus convection scheme is intertwined with other model weaknesses, and it is very difficult, if not impossible, to isolate one from the rest. However, assuming that the model employed for this investigation is sufficiently realistic, the results of the findings may not be significantly affected, even if future improvements change the moist processes in the model. This indeed was the case with several surface albedo, soil moisture, and surface roughness studies that were made before the development of the realistic biosphere model(s), such as SiB of Sellers et al. (1986), and the biosphere–atmosphere transfer scheme (BATS) of Dickinson et al. (1986). Nevertheless, it is a debatable assumption that may not hold for cumulus convection, particularly in view of the uncertainties in cumulus parameterizations of the present time. This becomes evident in the intercomparison of the current results with those of the earlier studies of Donner et al. (1982) and Ose et al. (1989).

4. Results

Two sets of simulations, one with and one without a cumulus scheme, were made with the GLA GCM. Each set contains three summer (June–August) integrations. The first set of integrations, comprising the control cases, were made with the GCM having a state-of-the-art cumulus scheme due to Arakawa–Schubert (ASCP). The control simulations are identified as WC (with cumulus convection) simulations. The second set of integrations, containing the experiment cases, are identified as NC (no cumulus convection) simulations. Nevertheless, identical dry-convective adjustment was present in both cases, and it includes mixing of heat, moisture, and momentum among all layers involved in the adjustment process. Such kinds of moisture and momentum mixing were not included in the earlier studies of Donner et al. (1982) and Ose et al. (1989), and it is emphasized that this difference in parameterization has produced some major variances between current and earlier results. The fundamental difference between moist-convective adjustment and dry-convective adjustment (which appear in the absence of cumulus convection) is that the latter ensues when the atmosphere is dry (and not moist) statically unstable, that is, the lapse rate exceeds the

dry lapse rate. Evidently, for a saturated atmosphere, the end product of dry-convective adjustment plus heating by supersaturation condensation can be very similar to that of the moist-convective adjustment; however, for drier conditions when the condensation does not occur, the dry adjustment produces dry-adiabatic lapse rate. The foregoing discussion indicates that in the moist tropics, particularly in the region containing the ITCZ, NC simulations may produce atmospheric lapse rates that are very similar to the moist lapse rates and are realistically produced by WC simulations.

All simulation experiments started from an initial-time atmosphere based on the analysis of observations; three different initial times that were 12-h apart starting from 0000 UTC 19 May 1988 were chosen. The same climatological boundary conditions—sea surface temperature, snow, ice, and vegetation—were used for both sets of integrations. The results are divided into two main parts: 1) hydrologic cycle differences and 2) circulation differences. An attempt is made to bring out all the important features that affect the hydrologic cycle and shed light on the differences in (i) surface fluxes, (ii) moisture transports, and (iii) zonal and/or regional circulation. In the following discussions, difference fields always imply NC-minus-WC fields unless specified otherwise.

a. Surface energy fluxes

In the ensemble time mean for June, July, and August (hereafter JJA time mean), the globally averaged solar radiation reaching the land is larger by about 4%, whereas the corresponding value for oceanic regions is about 6% larger (actual distributions are not shown). Since the SSTs are prescribed externally to the model, any changes in surface radiative fluxes over the oceans are immaterial for earth-atmosphere interactions. Nevertheless, for land the increases in solar radiation are fairly well distributed over the major continents, namely, North America, North Africa, Europe, and Asia, including the monsoonal regions of northern India. However, roughly half of this increase (about 2%) is mitigated by an increase in the outgoing longwave radiation at the surface. Thus, on the average, there is only about a 3.5 W m^{-2} increase in the net radiation at the land surface (NC-minus-WC) simulations; consequently, we do not see major changes in either the surface latent heat fluxes (Figs. 1a,b) or the sensible heat fluxes (not shown). Over many large continents where solar-radiation differences are larger (about 10 W m^{-2}) an increase in evaporation is noted. Despite an increase in the net radiation absorbed at the land surface, the global evaporation for NC simulations reduces slightly (as compared to WC simulations). This is a direct outcome of a 100% versus 90% relative humidity criterion for the onset of large-scale versus con-

vective rain. Finally, to balance the surface energy budget, the sensible heat flux increases. Although quite small and generally inconsequential as compared to the natural variability of climate, the simulated differences in surface fluxes in the tropical regions are more significant than those in extratropical regions; therefore, tropical regions will be the primary focus of this study.

b. Evaporation and precipitation differences

Figure 1a shows JJA time-mean evaporation fields for WC and NC integrations and the differences: NC minus WC; the evapotranspiration is roughly the same in both simulations except for the ITCZ region. The zonal-mean fields also reflect that the most conspicuous differences are over the tropical oceanic regions, Fig. 1b. This structure in the difference fields can be easily explained as follows. First, it was noted (not shown) that the net solar radiation reaching the land surface is slightly larger for NC simulations, whereas the vertical gradient of specific humidity in the boundary layer is somewhat larger in WC simulations. These are directly caused by reduced cloudiness and inefficient removal of water vapor from the boundary layer in NC as compared to WC simulations. Since these two aspects introduce small counteracting effects on land surface evaporation (LSE), it is reasonable to find that LSE is not too different in NC and WC simulations. Nevertheless, NC simulations do produce larger LSE over the eastern United States, Africa, and India (Fig. 1a, bottom panel). Second, the SSTs, which are externally prescribed, are kept identical in both experiments; however, as explained in section 4a, the boundary-layer specific humidity is larger in NC simulations; consequently, the ocean surface evaporation reduces. Thus, small reductions in the evaporation over tropical oceans, particularly in the monsoonal regions of the eastern Pacific, are related to relative humidity variations in the boundary layer produced by large-scale (convective) condensation requiring 100% (90%) relative humidity for the onset. The effect is evident in the tropical regions where the ocean surface evaporation, being a strong function of SSTs, is significant. The main point to note is that the changes in incoming solar radiation are quite small over land and virtually inconsequential over oceans. Therefore, the cloud-radiation feedback effect turns out to be rather trivial in this investigation. This is fortuitous as well as useful for this study because the differences in simulations are primarily caused by the changes in convectively induced condensation.

Figure 2a shows precipitation fields for JJA time mean: outside of the tropics the global precipitation is roughly the same in both heating simulations; and in the tropics the largest precipitation differences are noted. Specifically, large as well as statistically significant reductions (at 95% or higher confidence level, see Sud et al. 1991 for details of the calculations) in NC

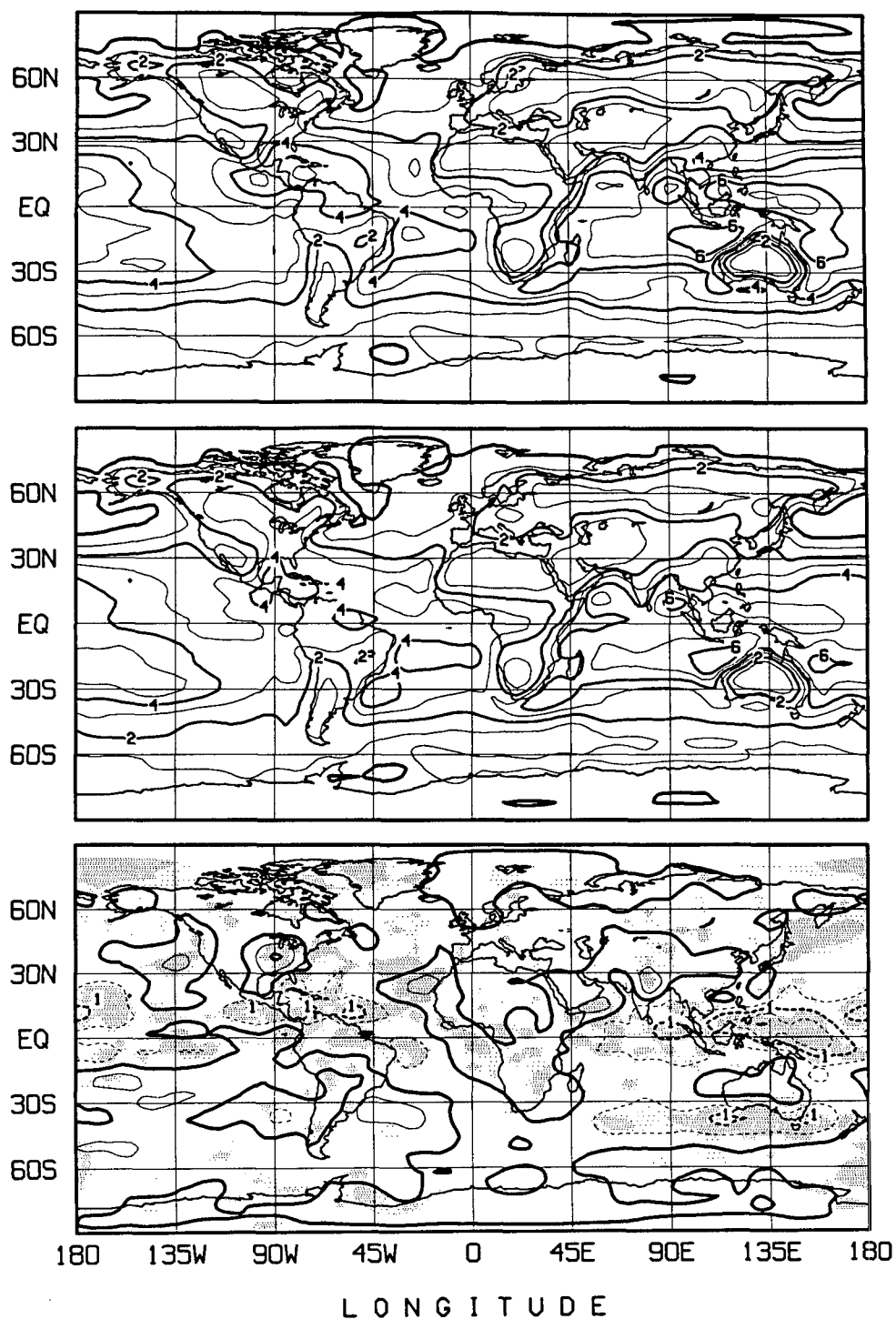


FIG. 1a. Evaporation (mm day^{-1}) for the ensemble mean for June, July, and August simulations. Top panel: control; middle panel: experiment; and bottom panel: experiment minus control. Regions showing 95% or better statistical significance in the differences are shaded. Contours 1, 3, 5 . . . are drawn thin, whereas 2, 4, 6 . . . are drawn thick.

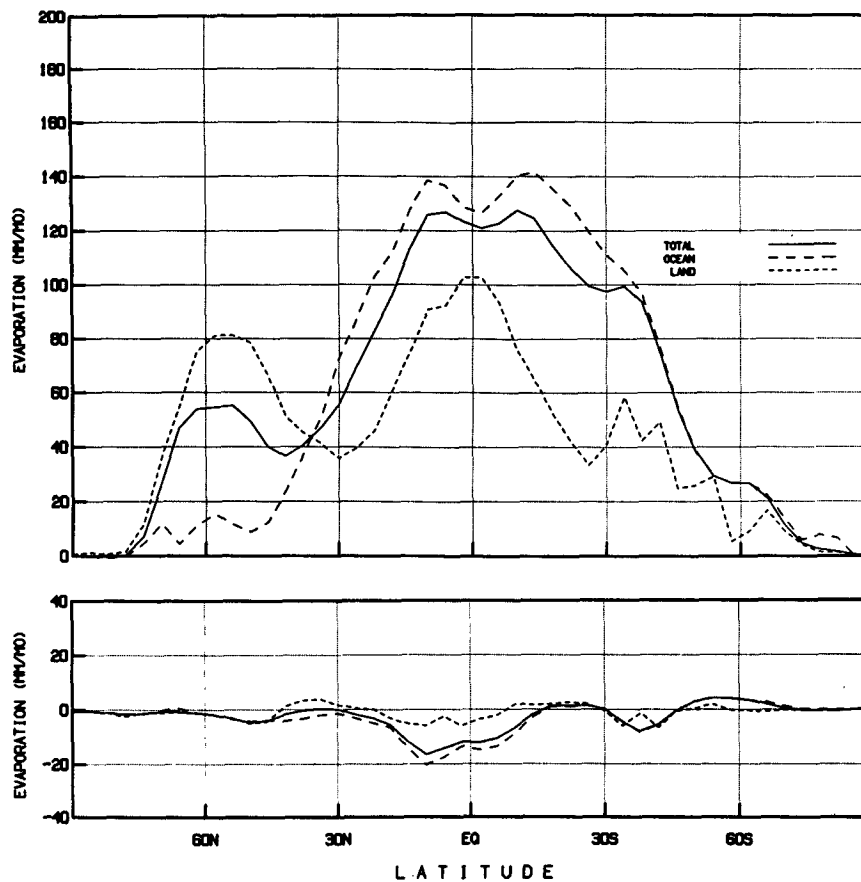


FIG. 1b. Zonal-mean evaporation (mm day^{-1}) for the ensemble mean for June, July, and August simulations. Top panel: control; and bottom panel: experiment minus control.

precipitation are found for Central and some parts of North America, and monsoonal regions of India and the maritime islands of tropical eastern Pacific. These are also regions of intense convective activity in the summer season; therefore, it is not surprising to find that the significant differences appear in these regions. There is an increase in rainfall over tropical North Africa (0° – 10°N). This happens because the subtropical high over the North Atlantic weakens, thereby weakening the low level easterlies into Amazonia while strengthening the moisture convergence by westerlies into tropical North Africa. Thus, moisture convergence into tropical North Africa is accompanied by moisture divergence from tropical South America. Garcia's (1985) satellite-derived monthly cloud data shows some teleconnectivity between Sahelian–African and Amazonia clouds; presumably, the observed teleconnectivity is related to the strength of the easterlies, which in turn is related to the strength of the subtropical high over the North Atlantic, as is the case in our simulation experiments. Since an efficient removal of moisture by convection in the WC simulation must

yield somewhat higher evaporation over the oceans, an increase in evaporation accompanying the increase in precipitation could be naturally expected in regions of intense convection. Here, too, the zonal precipitation fields show that the most conspicuous differences are over the tropical regions, Fig. 2b. The zonal average rainfall goes down over the ITCZ at about 10°N while increasing south of it at about 2°S . One can naturally expect changes in condensation heating to agree with changes in rainfall, but the cumulus convection can also affect the vertical heating profile, which in turn has a strong influence on the vertical temperature profile and motion fields. For the present study, this is evident in the magnitude of heating but it does not significantly affect the vertical structure of the heating profile as discussed in section 4d.

c. Moisture flux divergences

The moisture flux convergences for time-mean JJA simulations for the stationary and transient components for the boundary layer, as well as for the entire

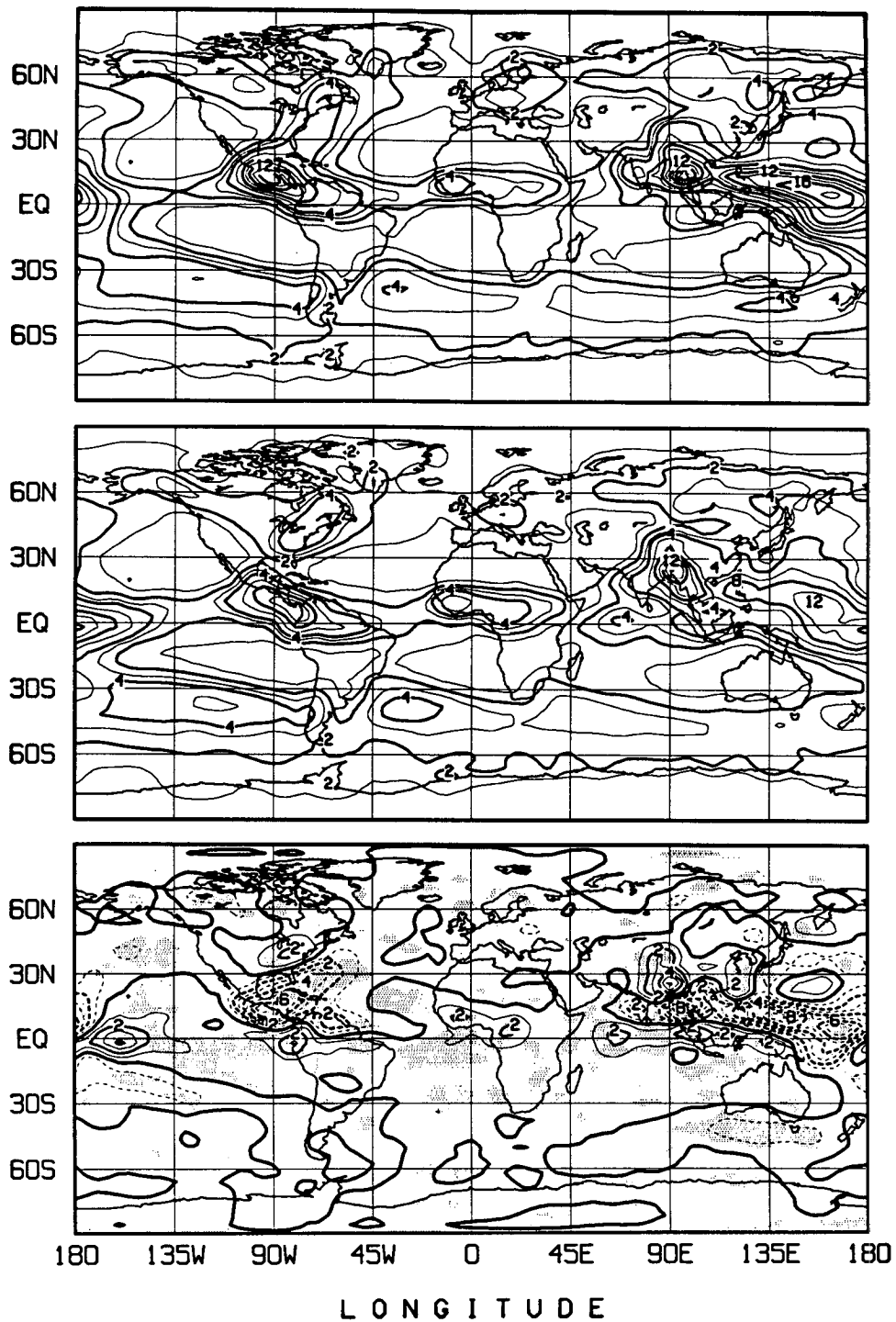


FIG. 2a. Precipitation (mm day^{-1}) for the ensemble mean for June, July, and August simulations. Top panel: control; middle panel: experiment; and bottom panel: experiment minus control. Regions showing 95% or better statistical significance in the differences are shaded. Contours 1, 3, 5 . . . are drawn thin, whereas 2, 4, 6 . . . are drawn thick. Negative differences are dashed.

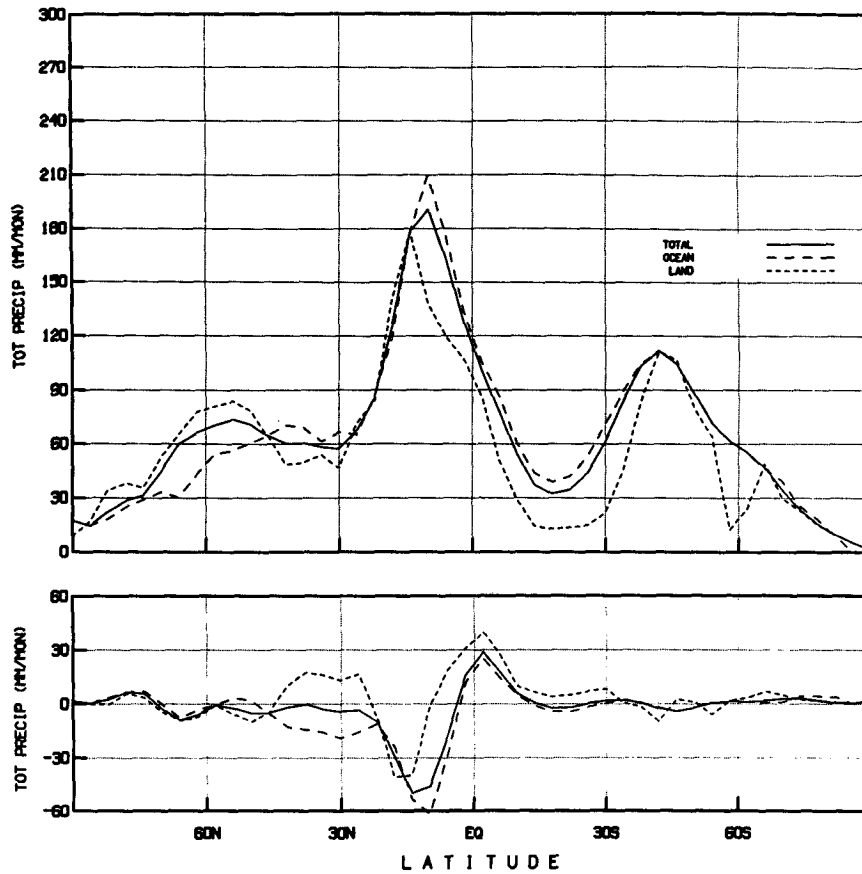


FIG. 2b. Zonal-mean precipitation (mm day⁻¹) for the ensemble mean for June, July, and August simulations. Top panel: control; and bottom panel: experiment minus control.

column atmosphere, can be calculated as follows. If we write $\mathbf{V} = \bar{\mathbf{V}} + \mathbf{V}'$ and $q = \bar{q} + q'$ where \mathbf{V} and q represent wind vectors and specific humidity, with overbars denoting the time mean, and prime denoting the departure from the time mean at a given location: i, j, k (dropped for brevity), then the horizontal moisture flux divergence in a sigma layer of thickness ΔP would be

$$\frac{\Delta P}{g} (\nabla \cdot \mathbf{V}q) = \frac{\Delta P}{g} (\nabla \cdot \bar{\mathbf{V}}\bar{q}) + \frac{\Delta P}{g} (\nabla \cdot \mathbf{V}'q'). \quad (1)$$

The total, horizontal water vapor flux divergence, as expressed on the right-hand side, contains two parts: the stationary (time-mean) part and the transient (eddy) part, as represented by the first and the second terms on the right-hand side of (1), respectively. It is found that the change in total, horizontal water vapor flux convergence (negative of divergence) in the boundary layer (represented by sigma layer 9 of the model) is almost entirely due to the stationary part of (1), as shown in Fig. 3. The transient part is not only statistically insignificant but it also contributes very lit-

tle to NC-minus-WC differences (not shown because all the values were smaller than $\pm 1.0 \text{ mm day}^{-1}$). This indicates that almost all the changes in circulation and rainfall are emanating from changes in the stationary component of boundary-layer water vapor flux convergence. Thus, absence of cumulus convection causes permanent change in the time-mean circulation pattern in the boundary layer, while the transient component of circulation, which is anyway weak in the boundary-layer region, contributes very little to it.

The results of similar calculations for the entire column atmosphere are given by (2):

$$\int_{\text{bot}}^{\text{top}} \frac{\Delta P}{g} (\nabla \cdot \mathbf{V}q) = \int_{\text{bot}}^{\text{top}} \frac{\Delta P}{g} (\nabla \cdot \bar{\mathbf{V}}\bar{q}) + \int_{\text{bot}}^{\text{top}} \frac{\Delta P}{g} (\nabla \cdot \mathbf{V}'q'). \quad (2)$$

The left-hand side of (2) gives the total water vapor flux divergence, as shown in Fig. 4a. It must equal precipitation minus evaporation, provided small changes

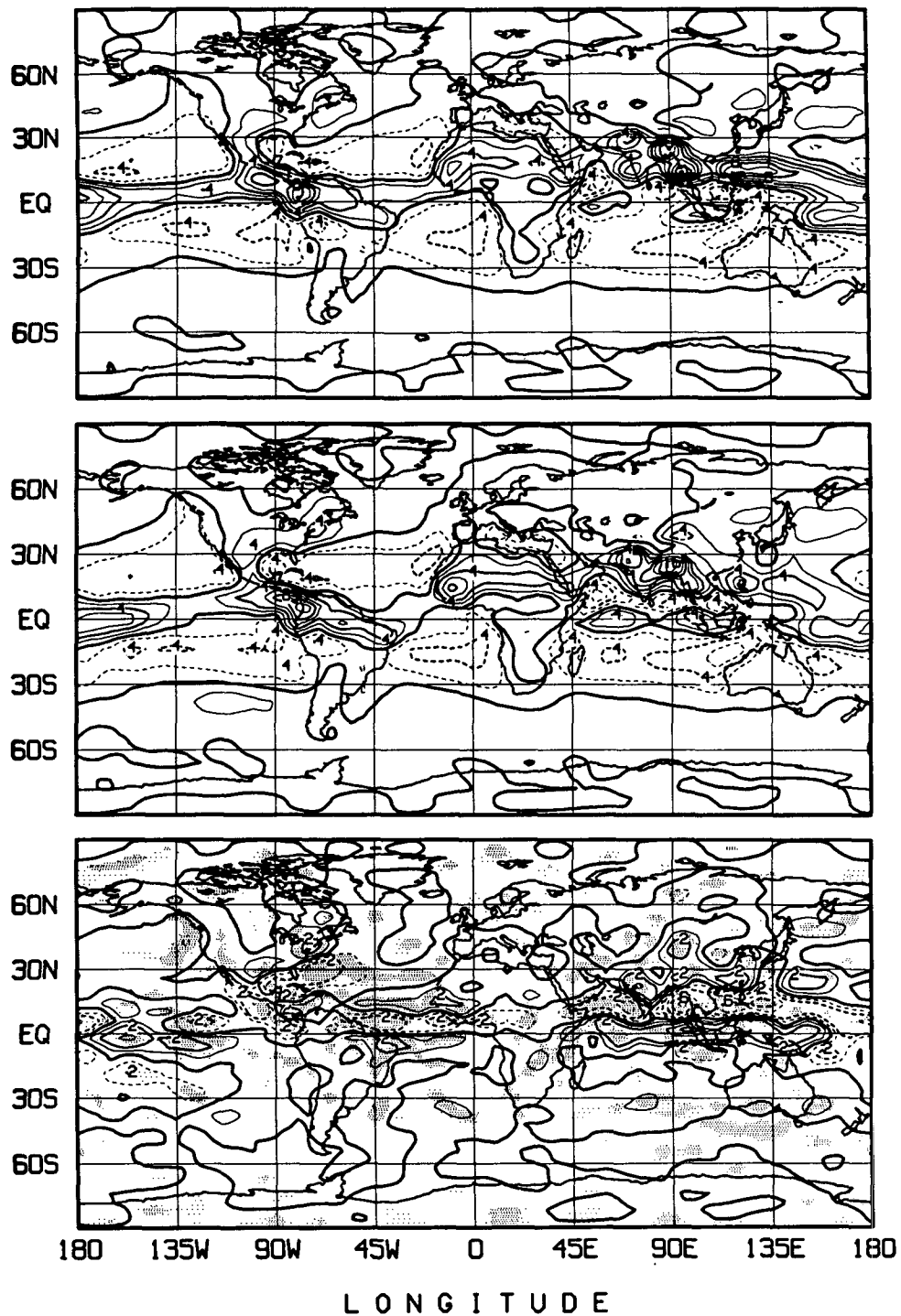


FIG. 3. Boundary-layer moisture flux transport convergence (mm day^{-1}) for the ensemble mean for June, July, and August simulations. Top panel: control; middle panel: experiment; and bottom panel: experiment minus control. Regions showing 95% or better statistical significance in the differences are shaded. Contours 1, 3, 5 . . . are drawn thin, whereas 2, 4, 6 . . . are drawn thick. Negative differences are dashed.

in the atmospheric water vapor storage can be neglected. The differences between stationary and transient parts of water vapor flux convergences (divergence with a negative sign) are shown in Fig. 4b. As compared to WC simulations, NC simulations not only yield reduced evaporation but also produce reduced water vapor flux convergence into the monsoonal regions of tropical eastern Pacific leading to reduced precipitation. This can be expected because, without cumulus convection, the removal of water vapor by condensation is relatively inefficient, which reduces (weakens) local diabatic heating as well as its dependant thermally driven convergence. Consequently, the rainfall along the monsoon trough and the ITCZ region, at about 10°N , reduces, whereas the rainfall south of the trough increases. The influence is particularly strong over the oceans, which leads to a north-south dipole in the difference fields of moisture flux convergence. Indeed, over land there is also some increase in rainfall north of the ITCZ and there is some east-west variability along with interesting patterns; these appear to be related to land-sea differences in surface fluxes and/or other effects such as orographic forcing in hilly regions of the Indian subcontinent, for example. The same is true for the monsoonal region of North America. The rainfall decreases locally while increasing southward.

d. Hadley circulation

The changes in the magnitude and structure of tropical diabatic heating are expected to directly affect the Hadley circulation. For the WC simulations, the Hadley cell is well simulated (Fig. 5), as compared to analysis of observations (Newell et al. 1972). The Hadley cell in the WC is somewhat stronger than in the NC simulations; tighter gradients in the mass flux at about 10°N indicate intense and somewhat deeper vertical rising motion. According to the diagnostic equation for the streamfunction for the mean meridional circulation (Holton 1972, p 230), reduced condensation heating in the tropics is consistent with a weaker Hadley cell. Although a weak Hadley cell in the tropics could be forced by meridional momentum and heat fluxes, even in the absence of condensation heating, but that does not apply to our NC simulations. Indeed, the sinking part of the Hadley cell and indirect Ferrel cell in the Southern Hemisphere are also stronger in WC simulations as compared to NC simulations. The strength of the Hadley cell in WC simulations is consistent with stronger convergence into the monsoonal regions together with larger surface evaporation in the tropics. This result is at variance with that of Donner et al. (1982). A logical reason for this discrepancy is that we have dry-convective mixing of heat moisture and momentum that the Donner et al. model did not have. Thus, for a given vertical temperature profile, our large-scale condensation heating produces the same

kind of overall effect in NC simulations that cumulus convection produces in WC simulations; this is further discussed in the following section.

On the other hand, the fact that only small differences in the rainfall exist despite some significant differences in the strength of the Ferrel cell is quite interesting. A larger moisture convergence at about 40° – 60°S , over the rising branch of the Ferrel cell in the WC simulation, is partly countered by a somewhat lower surface evaporation over the region; consequently, there is very little change in the rainfall (only about 5%). Recognizing that the rainfall in this region is only about 25% larger than the surface evaporation, an increase in moisture convergence in WC simulations, that is partly mitigated by a decrease in evaporation, can easily lead to a smaller change in the simulated rainfall. The lower evaporation of WC simulations is presumably a direct consequence of stronger surface winds of high relative humidity blowing poleward, leading to a decrease in the humidity gradient of the surface layer.

e. Diabatic and condensation heating

Figure 6a shows that convective-plus-large-scale condensation heating for WC simulations is much larger than that for NC simulations, particularly over the ITCZ region below the ascending branch of the Hadley cell. Surprisingly, the height of the level of maximum condensation heating over the ITCZ region is about the same for both simulations. In an earlier study, Sud et al. (1991) found that the large-scale convection with dry-convective mixing of heat and moisture momentum tends to mimic the moist convection, as if a resolved process over several time steps. The mechanism works as follows. First, large-scale condensation in a layer warms it; subsequently, if the warming was large enough to make the layer dry-convectively unstable with respect to the layer atop, upward mixing of heat, moisture, and momentum ensues as a result of dry-convective adjustment. This leads to a large increase in the relative humidity atop because each of the fully mixed layers must have the same specific humidity at the end of the adjustment. This moisture increase in the upper layer leads to a supersaturation condition producing large-scale condensation and heating. Thereafter, the cycle repeats, affecting the next higher level. The process continues until depletion of moisture makes the condensation heating within the layer so small that it does not become dry-convectively unstable. Thus, large-scale condensation heating, which replaces cumulus heating, ends up mimicking cumulus convection transporting heat and moisture, as well as momentum, aloft. In the earlier versions of the model where the dry-convective adjustment only mixed heat but not moisture and momentum, such a similarity in condensation heating among simulations with and

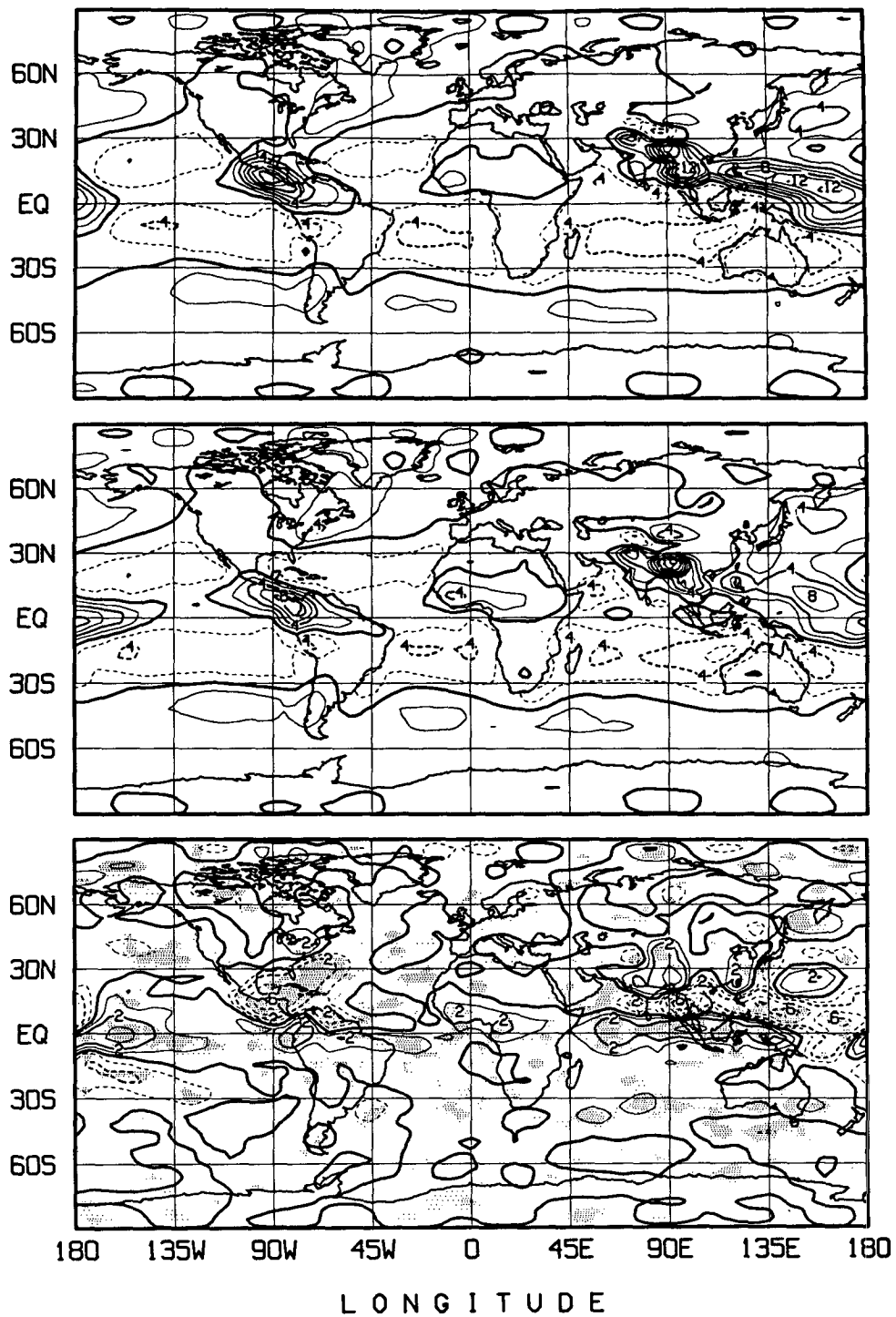


FIG. 4a. Total-column atmosphere moisture flux transport-convergence (mm day^{-1}) for the ensemble mean for June, July, and August simulations. Top panel: control; middle panel: experiment; and bottom panel: experiment minus control. Regions showing 95% or better statistical significance in the differences are shaded. Contours 1, 3, 5 . . . are drawn thin, whereas 2, 4, 6 . . . are drawn thick. Negative differences are dashed.

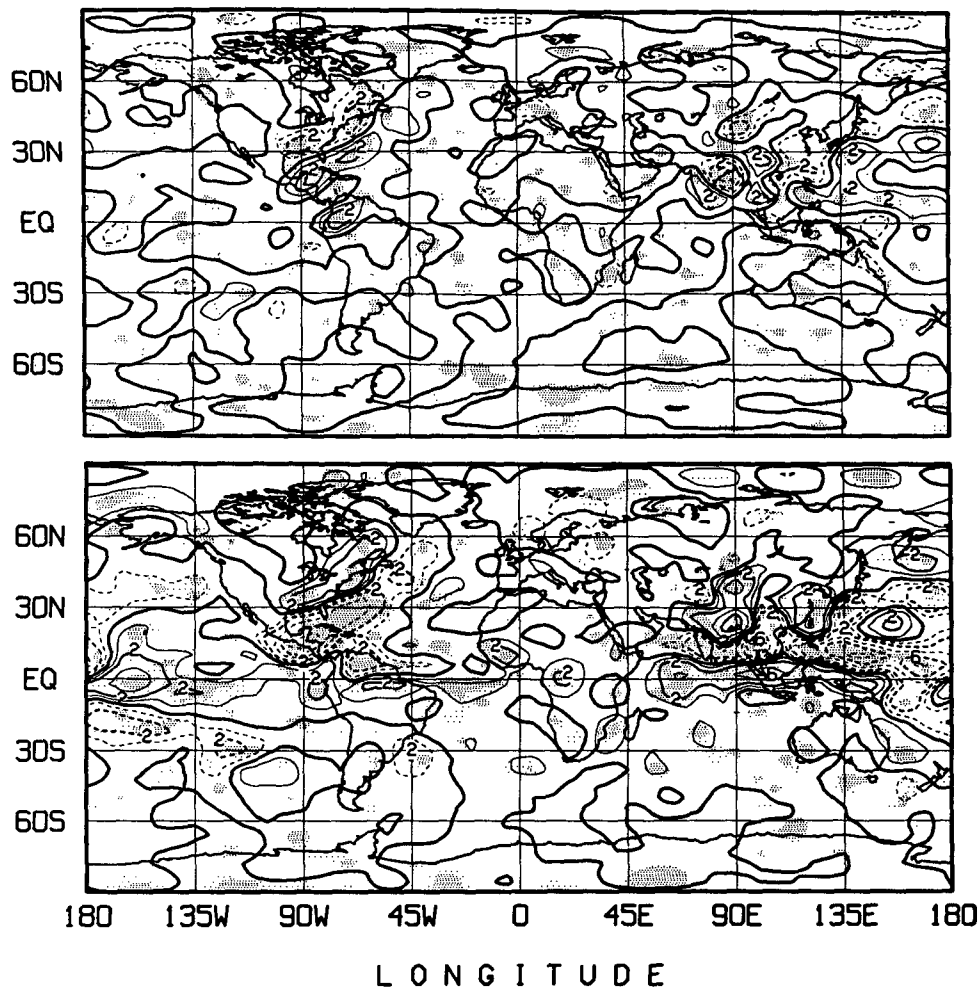


FIG. 4b. Total-column atmosphere moisture flux transport-convergence differences (mm day^{-1})—experiment minus control—for the ensemble mean for June, July, and August simulations. Top panel: transient part; and bottom panel: stationary part. Regions showing 95% or better statistical significance in the differences are shaded. Contours 1, 3, 5... are drawn thin, whereas 2, 4, 6... are drawn thick. Negative differences are dashed.

without cumulus convection was not noted; this is also evident in Donner et al. (1982) and Ose et al. (1989) experiments. Therefore, an analysis of the present experiments reveals a mechanism by which the dry-convective adjustment, together with large-scale condensation heating, tend to mimic cumulus convection, but in a relatively inefficient way as discussed in Sud et al. (1991). Indeed, as pointed out earlier, the decrease in condensation heating in the ITCZ region for NC simulations leads to a reduced convergence locally; consequently, the convergence increases upstream (southward) of the flow, thereby producing an increase in rainfall south of the ITCZ region; this is noted in the zonal as well as global plots of condensation heating and rainfall fields. The NC condensation heating fields also show more heating in the lower troposphere as

compared to WC condensation heating fields. Positive heating differences (NC minus WC) can be noted throughout below the 900-mb level.

The corresponding plots for zonal-average diabatic heating are shown in Fig. 6b. Radiative flux transport divergences produce atmospheric cooling in the clear regions of subtropical highs and over the South (winter) Pole. The radiative cooling weakens the tropical condensation heating structures without making any major changes in them; consequently, the difference fields of zonal- and time-mean diabatic heating are similar to the corresponding condensation-heating-field differences. One can explain large gradients in radiative heating structures by including the cloud-radiative interactions (not shown). Although we have calculated and examined differences in radiative, sensible, and

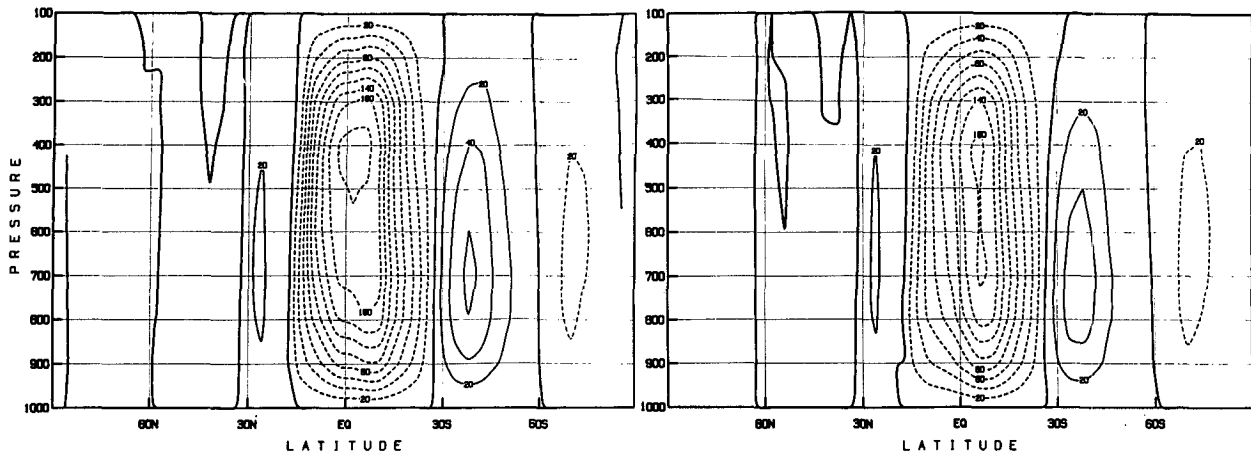


FIG. 5. Mean meridional circulation (10^9 kg s^{-1}) for the ensemble mean for June, July, and August simulations. Left panel: control simulation; and right panel: experiment simulation.

total diabatic heating fields at 200-, 500-, and 850-mb levels, they are not shown here because there is very little information in them. However, a few relevant remarks must be made. Namely, the differences in surface sensible and net surface radiative fluxes were relatively small, and that the differences in diabatic heating fields roughly mimic the condensation heating fields differences.

f. Streamfunctions at the 850- and 200-mb levels

Figure 7 shows JJA time-mean NC-minus-WC differences in the streamfunction fields; shaded regions represent 95% or better statistical significance of the difference fields. The 850-mb-level differences (Fig. 7, top) show westerlies into tropical Africa; it represents weakening of strong easterlies at the equator and strengthening of westerlies at about 10°N . Similarly, a weakening of westerlies in the tropical Indian and western Pacific ocean region shows as easterlies in the difference fields. Hence, it can be inferred that the tropical as well as extratropical circulation, that is, the wind fields weaken in response to reduced condensation heating for NC (as compared to WC) simulations. The influence in the extratropical regions is also consistent; the 850-mb winds in the subtropical highs show significant weakening over the North and South Atlantic regions. If one primarily concentrates on the regions where the differences are statistically significant, it is evident that the wind magnitudes (NC-minus-WC differences) have reduced in each case.

The 200-mb streamfunction differences (Fig. 7, bottom) show that the winds at this level are generally weaker in the NC as compared to the WC simulations. However, there is no clear (one-to-one) correspondence between the wind structures of the two sets of simulations as is the case for 850-mb analysis. Consequently,

the difference fields show complex structures that are statistically significant at 95% confidence level. In general, there is a weakening of strong stationary flow regimes; for example, westerlies in the region of $30^\circ\text{--}60^\circ\text{S}$ and $30^\circ\text{--}60^\circ\text{N}$ weaken significantly showing easterlies in the differences; westerly winds between Amazonia and tropical Africa also weaken again showing easterlies in the difference fields. Correspondingly, there is a weakening of the Walker circulation that is indicated by the weakening of easterlies at about 90°E as well as weakening of the westerlies at about 45°W at 200-mb level over the equator (Fig. 6). This picture is consistent with a weaker ITCZ in the tropics. Moreover, the structure above the subtropical high over the North and South Atlantic is complex because there is a significant displacement along with weakening of the strong winds at that level. Nevertheless, there is clear evidence of generally weaker and less energetic circulation over North and South America, Africa, and southern Asia; even though the picture in some of these regions, depicting a shift in the circulation patterns, is somewhat harder to understand and interpret.

g. Zonal-mean differences in temperature, relative humidity, and winds

Figure 8 shows NC-minus-WC differences in the zonal-mean JJA time-mean fields. The zonal-mean temperature differences are negative almost everywhere, with the largest difference of about 4° at about 400-mb level. This is due to the influence of reduced condensation heating and reduced cloudiness in NC simulations. The OLR cooling does have a strong influence because changes in condensation heating alone could not produce such large zonal temperature differences, particularly over the South Pole. Although WC simulations produce higher specific humidity, ex-

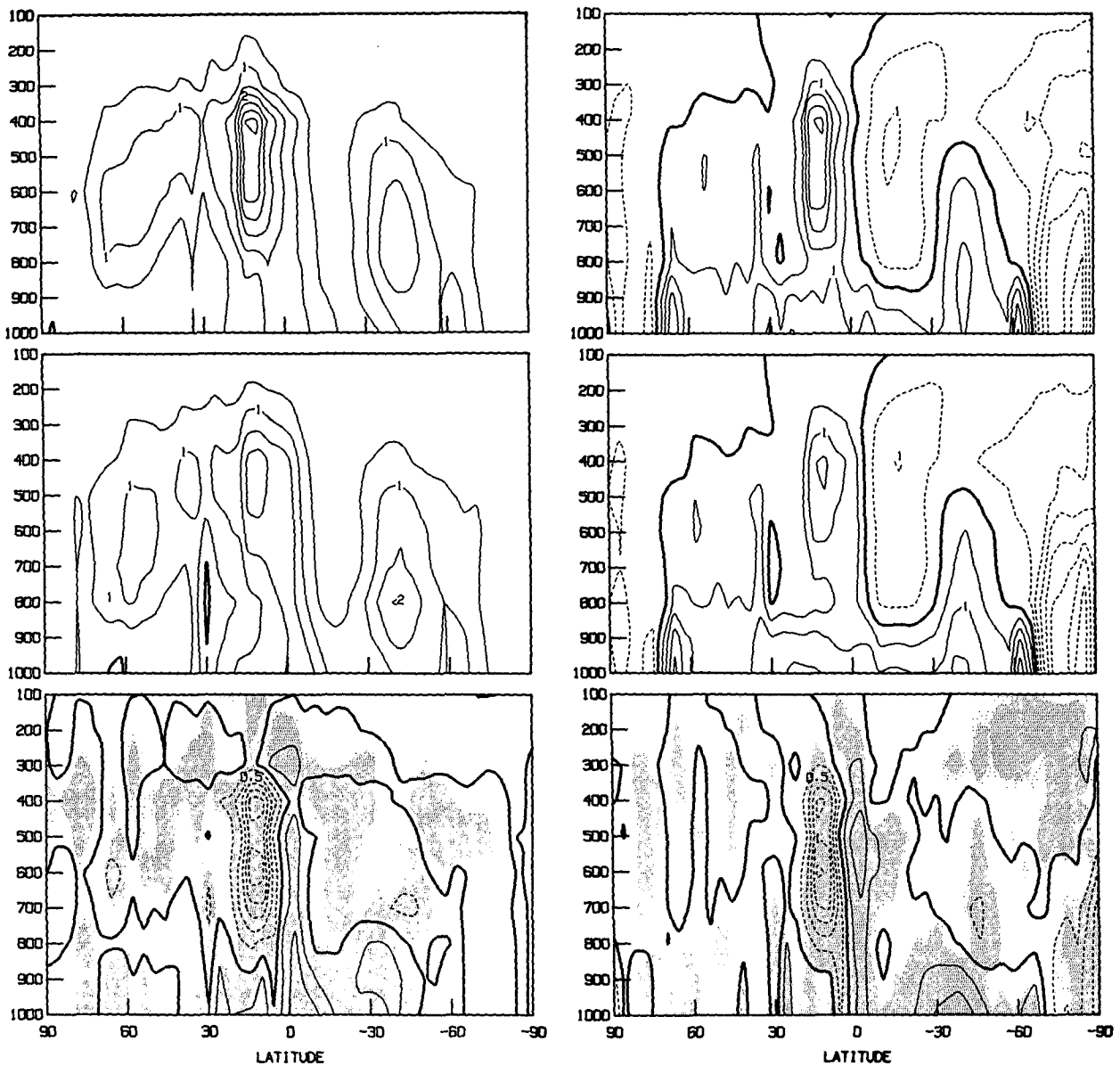


FIG. 6. (a) Zonal-mean condensation heating (K day^{-1}) for the ensemble mean for June, July, and August simulations. Top panel: control; middle panel: experiment; and bottom panel: experiment minus control. Regions showing 95% or better statistical significance in the differences are shaded. Negative differences are dashed. (b) Zonal-mean total diabatic heating (K day^{-1}) for the ensemble mean for June, July, and August simulations. Top panel: control; middle panel: experiment; and bottom panel: experiment minus control. Regions showing 95% or better statistical significance in the differences are shaded. Negative differences are dashed.

cept at 400-mb level, the relative humidity differences that take the temperature change effect into account, reduce in the lower troposphere. This may appear paradoxical but it is easy to understand; evidently, the moisture structure of the large scale is produced by large-scale condensation and dry convection in NC simulations. The zonally averaged V -wind differences are significant in the tropics and reflect weaker Hadley and southern Ferrel cells. This has been already seen

in the Hadley cell comparisons in section 4d. The zonally averaged U -wind differences also show weaker circulation for the NC simulation: weaker easterlies in the tropics and westerlies in the extratropics. Although some of the differences are quite small, the shading shows that they are statistically significant at 95% or better confidence levels.

The zonal-mean time-series differences (not shown) in the temperature and humidity fields for the tropical

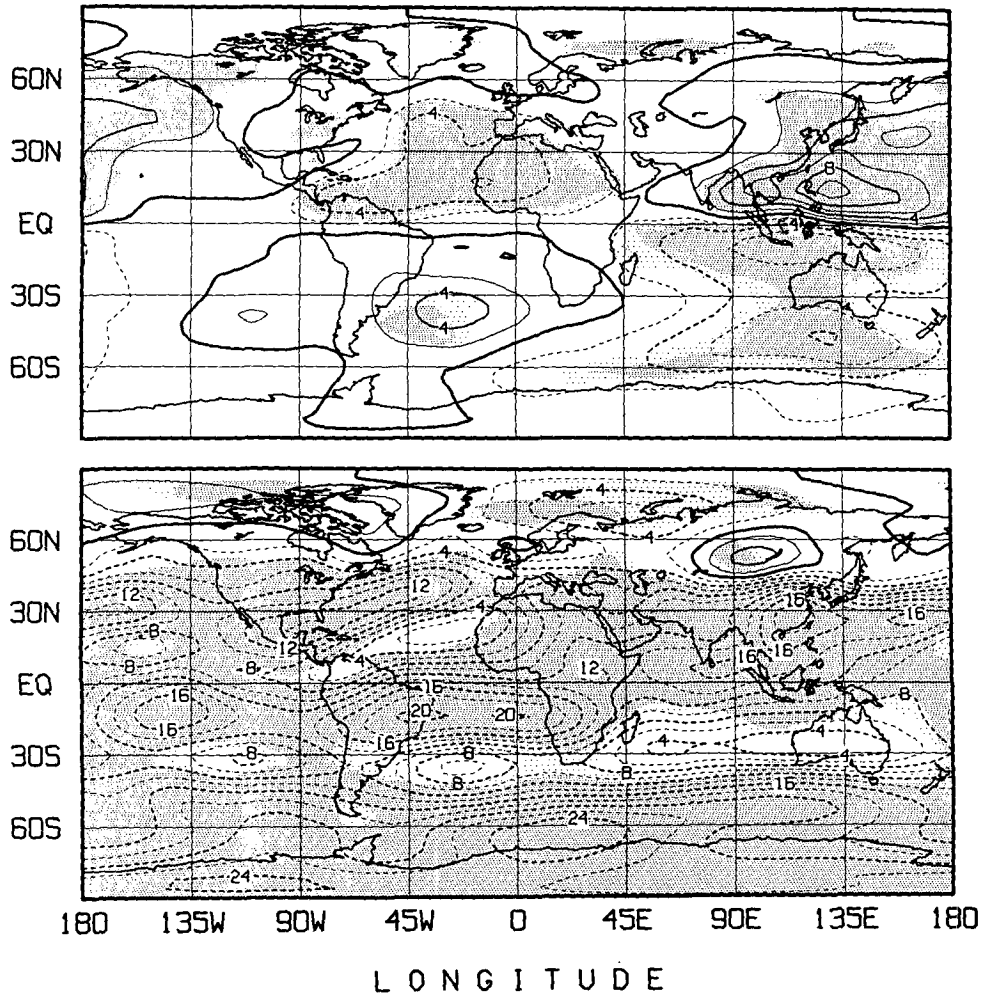


FIG. 7. Experiment-minus-control difference fields of streamfunction in units of $10^6 \text{ m}^2 \text{ s}^{-1}$ at 850-mb level (top panel) and 200-mb level (bottom panel) for the ensemble mean for June, July, and August simulations. Regions showing 95% or better statistical significance in the differences are shaded. Negative differences are dashed.

(20°N – 20°S) atmosphere were further examined in the last 92 days of the simulation experiments. It shows cooler conditions for NC as compared with WC simulations. This result is again at variance with that of Donner et al. (1982), who show that cumulus convection warms the upper levels and cools the lower levels. Indeed, the vertical heating distribution of ASCP is quite different from that of Kuo's convection scheme (Geleyn et al. 1982); therefore, some large differences can naturally be expected. Evidently, the GLA GCM with ASCP produces much better vertical heating distribution (Figs. 6a,b) in the tropics as compared with the European Centre for Medium-Range Weather Forecasts (ECMWF) model tests by Geleyn et al. (1982). We believe either our model improvements are the backbone of this much better performance of ASCP in the GLA model, or there are some other fun-

damental problems with the Geleyn et al. (1982) implementation of ASCP in the ECMWF model. Regardless, there is some drying in the model and we hope to eliminate it in the future version of the GLA GCM by including cooling and moistening due to cumulus-induced downdrafts, following Cheng (1989) and Cheng and Arakawa (1990). Therefore, at this point, it is difficult to state unequivocally whether the present results that show uniform cooling throughout the atmospheric column for NC simulations is more realistic or not, as compared to Donner et al. (1982). The corresponding time series for water vapor show lower specific humidity (figure not shown) in NC simulations as compared with WC. This can be naturally expected with the cooler atmosphere. The only exception being the 400-mb level (sigma level 4 of the model) that is somewhat drier for WC simulations despite a

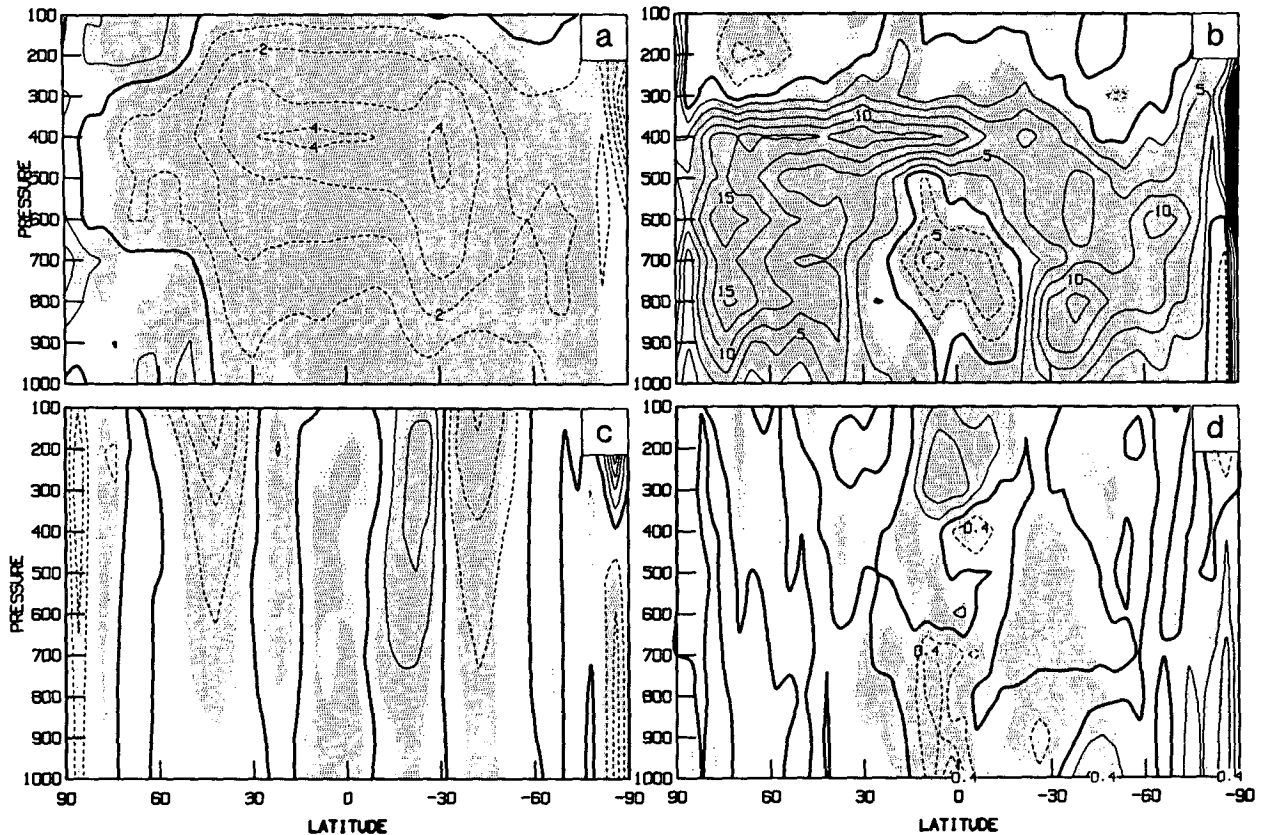


FIG. 8. Experiment-minus-control differences for zonal-mean values of the ensemble mean for June, July, and August simulations. The figure has four parts showing: (a) temperature (K); (b) relative humidity; (c) zonal winds (m s^{-1}); and (d) meridional winds (m s^{-1}). Negative differences are dashed.

4°C warming at that level. A drying in the WC simulation at 400-mb level is presumably related to sinking of dry air from aloft (in the large-scale environment), in response to deep cumulus convection. It is evident that deep cumulus-cloud plumes, which are parameterized to entrain exponentially growing mass (as a function of height) of environmental air, produce some drying below the detrainment level of the model. This is a very interesting result because it reveals the role of convection for drying the upper levels of the atmosphere. Its implications for GCM simulation experiments, with doubled atmospheric carbon dioxide (CO_2), may be that of a smaller positive feedback effect of water vapor on the radiative warming, in response to some upper-level drying that could be produced by an invigorated cumulus convection.

5. Summary and discussion

The role of cumulus convection in maintaining the global circulation and hydrologic cycle is examined by comparing two sets of ensembles, each containing three summer—June, July, and August—simulations. One set is made with and the other set is made without

cumulus convection in the model. The particular cumulus convection scheme is due to Arakawa-Schubert (1974) with some modifications by Sud et al. (1991). The results show the following:

- 1) A cumulus convection scheme makes a significant difference in the intensity of the tropical circulation, particularly in the ITCZ region where cumulus convection is strong. The largest differences appear in the monsoonal regions over India, Africa, and North America. The picture becomes very clear in the zonal-average fields that show that the Hadley cell, in the simulations without cumulus convection, is significantly weaker. This is consistent with significantly reduced condensation as well as diabatic heating over the ascending branch of the Hadley circulation (cell). The discrepancies between these results and those of an earlier study by Donner et al. (1982) are due to the differences in the cumulus schemes and other physical parameterizations, particularly the dry convection, of the model.

- 2) The decrease in the ITCZ rainfall in NC simulations, as compared with WC simulations, is largely compensated by an increase in rainfall north and south

of the ITCZ; this also shows clearly in the zonal-mean diabatic as well as condensation heating differences. A weaker tropical circulation (as inferred from weaker Hadley and Walker circulations) produced by lack of cumulus convection, weakens the winds reducing ocean evaporation as well as moisture convergence into the monsoon trough; together with condensation heating reductions, this produces a strong influence on the magnitude of condensation heating and water vapor distribution in the vertical. In this way cumulus convection affects tropical temperature and rainfall, including the hydrologic cycle itself.

3) Absence of cumulus convection does not appreciably lower the height of condensation heating. This happens because the dry-convective mixing of moisture transports the moisture up where it condenses as large-scale rain. Thus, instead of cumulus convection helping to transport the moisture to the level of neutral buoyancy and producing condensation heating, disallowing cumulus convection produces heating by large-scale condensation followed by moisture and heat transport by dry convection in sequential steps. This shows that large-scale condensation heating together with dry-convective mixing are roughly equivalent to resolving the grid-scale influence of moist convection. The main difference being that large-scale condensation deposits more heat at the PBL levels and much less at the upper levels.

4) The southern Ferrel cell for WC simulations is stronger than that for NC simulations. We believe that the strength of this cell reflects: (i) the influence of some convection in the region of 40°–60°S, and (ii) the indirect effect of a stronger Hadley cell in the tropics. Therefore, we infer that this result is internally consistent. Although the rainfall below the rising branch of the Ferrel cell also increases, the amount is insignificant as compared to the natural variability of the region. We find that the differences, as seen in the zonally averaged rainfall, are real but small because increased moisture convergence in the region is accompanied by reduced evaporation.

5) Without cumulus convection, the specific humidity is high in the boundary-layer region, but that is clearly the result of choosing a 90% relative humidity limit for the onset of moist convection, as compared with a 100% relative humidity limit for the onset of large-scale condensation. The zonal-mean tropical rainfall for the no cumulus convection simulations is less than that for the control cases with cumulus convection.

6) The similarity between condensation heating patterns for cumulus and no-cumulus convection simulations suggests that the large-scale condensation parameterization together with dry-convective adjustment mimics cumulus convection in the tropics, though inefficiently. We consider this as a very desirable feature of the current implementation of moist pro-

cesses because if the horizontal resolution of the model were to be increased to a scale at which cumulus convection is resolved, and cloud-plume mixing into the environment was physically determined by a turbulence scheme such as Mellor–Yamada 2.5 (which will produce significantly less mixing as compared to dry-convective adjustment), all one has to do is to disable the redundant cumulus convective parameterization because the model has the ability to resolve cumulus convection. Naturally, simulating cumulus convection, as well as its heating and moistening effects in a high-resolution model, is a limiting test of the physical parameterizations for a model.

Acknowledgments. Professor Issac Held of GFDL, in his capacity as editor of the *Journal of the Atmospheric Sciences*, suggested submittal of this investigation as a separate paper. The authors would like to thank Dr. Milton Halem and F. Shaffer at NASA's High Speed Computing Facility for making the ETA-10 machine time available at no cost; without the computing support, it would not have been possible to conduct these experiments. Thank are also due to Ms. L. Rumberg for support with graphics. This research is supported by the Land and Climate Program offices of NASA headquarters.

REFERENCES

- Arakawa, A., and W. H. Schubert, 1974: Interaction of cumulus cloud ensemble with the large-scale environment, Part I. *J. Atmos. Sci.*, **31**, 674–701.
- Cheng, M.-D., 1989: Effects of downdrafts and mesoscale convective organizations on heat and moisture budget of tropical cloud clusters. Part I and II. *J. Atmos. Sci.*, **46**, 1517–1564.
- , and A. Arakawa, 1990: Inclusion of convective downdrafts in the Arakawa–Schubert cumulus parameterization. Internal Tech. Rep., Department of Atmospheric Science, University of California, Los Angeles.
- Chou, M.-D., 1986: Atmospheric solar heating rate in the water vapor bands. *J. Atmos. Sci.*, **25**, 1532–1542.
- Dickinson, R. E., A. Henderson-Sellers, P. J. Kennedy, and M. F. Wilson, 1986: Biosphere Atmosphere Transfer Scheme (BATS) for the NCAR Community Climate Model. NCAR Tech. Note TN275, 68 pp.
- Donner, L. J., H.-L. Kuo, and E. J. Pitcher, 1982: The significance of thermodynamic forcing by cumulus convection in a general circulation model. *J. Atmos. Sci.*, **39**, 2159–2181.
- Garcia, O., 1985: Atlas of highly reflective clouds for the global tropics: 1971–1983. U.S. Department of Commerce, National Oceanic and Atmospheric Administration, Environmental Research Laboratories, Boulder, 365 pp. [NTIS PB87-129169.]
- Geleyn, J.-F., C. Girard, and J.-F. Louis, 1982: A simple parameterization for moist convection for large-scale atmospheric models. *Beitr. Phys. Atmos.*, **55**, 325–334.
- Geller, M. A., Y. C. Sud, H. M. Helfand, and K. Takano, 1988: Sensitivity of climatic response in a GCM to the selection of a cumulus parameterization scheme. *Tropical Rainfall Measurements*, John S. Theon and N. Fugono, Eds., A. Deepak Publishing, 57–68.
- Helfand, H. M., 1979: The effect of cumulus friction on the simulation of January Hadley circulation by the GLAS general circulation model. *J. Atmos. Sci.*, **36**, 1827–1843.
- Kalnay, E., R. Balgovid, W. Chao, D. Edelmann, J. Pfendner, L. Takacs, and K. Takano, 1983: Documentation of the GLAS

- Fourth-Order General Circulation Model. NASA Tech. Memo. 86064. Vol. 1, Goddard Laboratory for Atmospheres, NASA/Goddard Space Flight Center, Greenbelt, MD. [NTIS N8424048.]
- Kuo, H.-L., 1974: Further studies of the properties of cumulus convection on the large scale flow. *J. Atmos. Sci.*, **31**, 1232–1240.
- Lacis, A., and J. E. Hansen, 1974: A parameterization for the absorption of solar radiation in the earth's atmosphere. *J. Atmos. Sci.*, **31**, 118–133.
- Newell, R. E., J. W. Kidson, D. J. Vincent, and G. J. Boer, 1972: *The General Circulation of the Tropical Atmosphere and Interactions with Extratropical Latitudes*. Vol. I. The Colonial Press Inc., 258 pp.
- Ose, T., T. Tokioka, and K. Yamazaki, 1989: Hadley circulation and penetrative cumulus convection. *J. Meteor. Soc. Japan*, **67**, 605–619.
- Sellers, P. J., Y. Mintz, Y. C. Sud, and A. Dalcher, 1986: A simple biosphere model (SiB) for use within general circulation models. *J. Atmos. Sci.*, **43**, 505–531.
- Slingo, J., and B. Ritter, 1985: Cloud prediction in the ECMWF model. Tech. Rep. No. 46, European Centre for Medium-Range Weather Forecasts, Reading, England, 48 pp.
- Sud, Y. C., and J. Abeles, 1980: A non-iterative calculation for surface temperature and surface fluxes in the GLA GCM. NASA Tech. Memo. No. 80650, 13 pp. Goddard Laboratory for Atmospheres, NASA/Goddard Space Flight Center, Greenbelt, MD. [NTIS N8129697.]
- , and A. Molod, 1988: The roles of dry convection, cloud-radiation feedback processes and the influence of recent improvements in the parameterization of convection in the GLA GCM. *Mon. Wea. Rev.*, **116**, 2366–2387.
- , and G. K. Walker, 1990: A review of recent research on the improvement of physical parameterizations in the GLA GCM. NASA Tech. Memo. 100771, 64 pp. [Available from Goddard Laboratory for Atmospheres, NASA/Goddard Space Flight Center, Greenbelt, MD 20771.]
- , W. C. Chao, and G. K. Walker, 1991: Contribution to the implementation of Arakawa–Schubert cumulus parameterization scheme in the GLA GCM. *J. Atmos. Sci.*, **48**, 1573–1586.
- Wu, M. L. C., 1980: The exchange of infrared radiative energy in the troposphere. *J. Geophys. Res.*, **85**, 4084–4090.
- , and J. Susskind, 1990: Outgoing longwave radiation computed from HIRS2/MSU soundings. *J. Geophys. Sci.*, **95**, 7579–7602.